International Journal of Coal Geology 121 (2014) 123–128

Contents lists available at ScienceDirect

International Journal of Coal Geology

journal homepage: www.elsevier.com/locate/ijcoalgeo

Molecular simulation and experimental characterization of the nanoporous structures of coal and gas shale

Mahnaz Firouzi [a], Erik C. Rupp [a], Corey W. Liu [b], Jennifer Wilcox [a,*]

[a] Department of Energy Resources Engineering, Stanford University, Stanford, CA 94305-2220, USA
[b] Stanford Magnetic Resonance Laboratory, School of Medicine, Stanford University, Stanford, CA 94305-2220, USA

ARTICLE INFO

Article history:
Received 10 July 2013
Received in revised form 5 November 2013
Accepted 6 November 2013
Available online 13 November 2013

Keywords:
Characterization
Molecular modeling
Gas adsorption isotherm
NMR cryoporometry
Coal
Shale

ABSTRACT

Characterization of coal and shale is required to obtain pore size distribution (PSD) in order to create realistic models to design efficient strategies for carbon capture and sequestration (CCS) at full scale. Proton nuclear magnetic resonance (NMR) cryoporometry and low-pressure gas adsorption isothermal experiments, conducted with N_2 at 77 K over a P/P_0 range of 10^{-7} to 0.995, were carried out to determine the PSD and total pore volumes to provide insight into the development of realistic simulation models for the organic matter comprising coal and gas shale rock. The PSDs determined on the reference materials (SiliaFlash F60 and Vycor 7930) show a reasonable agreement between low-pressure gas adsorption and NMR cryoporometry showing complementarity of the two independent techniques. The PSDs of coal and shale samples were determined with low-pressure gas adsorption isothermal experiments, but were unable to be measured by NMR cryoporometry. This is likely due to a combined size and pore surface chemistry effect that prevents the water from condensing in the pores, such that when the sample is heated there is no distinction based upon melting or phase change. Molecular modeling is carried out to create the pore structure network in which the transport and adsorption predictions are based. The three-dimensional (3D) pore network, representative of porous carbon-based materials, has been generated atomistically using the Voronoi tessellation method. A comparison of the computed PSD using this method was made to the measured PSD using isothermal low-pressure gas adsorption isothermal experiments on coal and gas shale samples. Applications of this work will lead to the development of more realistic 3-D models from which enhanced understanding of gas adsorption and transport for enhanced methane recovery and CO_2 storage applications can be developed.

1. Introduction

The effect of increasing atmospheric CO_2 concentration on climate change is recognized as one of the most important environmental concerns (IPCC, 2007; White et al., 2005). Carbon capture and sequestration is one strategy that could potentially mitigate gigatons (Gt) of CO_2 emissions per year; however, technical and policy obstacles have thus far hindered wide-scale deployment of this strategy (Wilcox, 2012). To design efficient and reliable strategies for either carbon capture or sequestration at the full-scale, one needs to understand the chemical and physical properties of CO_2 and its interaction with its local surroundings at the molecular-scale. To investigate these properties, characterization studies need to be carried out alongside theoretical modeling efforts. Integration of theory and experiments will allow for the relevant physics at the molecular-level to be revealed. Determining the transport of CO_2 within the model systems can be used to understand the complex pore matrices of coal and gas shale that are important to determining their potential for CO_2 storage.

Coals and gas shale rocks are structural and chemical heterogeneous porous materials with porosity and PSDs varying throughout. For instance, a three dimensional chemical representation of a coal macromolecule based on data from physiochemical analyses was developed by Faulon et al. (1993). Pores in coal vary in size from microns to angstroms in dimension and cleat-fractures. A significant proportion of their total open pore volume is located in micropores of less than 20 Å pore size (Sharkey and McCartney, 1981; Wang et al., 2007). The pore size is classified into three pores: macropores which are larger than 500 Å, mesopores which are between 20 and 500 Å, micropores which are less than 20 Å (IUPAC, 1972). Quantifying PSD, pore connectivity and porosity is desirable to determine the difference between how gases such as methane and CO_2 are stored and permeate in the coal seams and shale formations (White et al., 2005). Hence, there is great interest in methods for measuring PSD and characterization of the porous structures previously discussed, which is the focus of this work from both theory and experiment.

Transport and adsorption properties of CO_2 and methane in the organic matrix of coal and gas shale rocks are strongly influenced, and sometimes even dominated by the morphology of their structure, which consist of the connectivity of pores, and their sizes, shapes and

* Corresponding author.
E-mail address: jen.wilcox@stanford.edu (J. Wilcox).

0166-5162/$ – see front matter © 2013 Elsevier B.V. All rights reserved.
http://dx.doi.org/10.1016/j.coal.2013.11.003

surface characteristics. The main source of heterogeneity for coal and shale rock is the complicated porous structure that cannot be represented by a single pore, as it contains pores of different shapes and sizes, including straight and tortuous pathways, and contracting and diverging channels. When such single pores are connected, they form pore networks. The realistic simulation of porous materials addresses two prominent aspects, namely, the modeling of the solid material itself and the generation of its pore structure including pore-size distribution and pore-network connectivity. The most direct route towards addressing both of these aspects is through the atomistic simulation of these materials. To properly address the representation of the morphology of these complicated structures, in the present work we describe an efficient molecular pore-network model for porous materials, and particularly of carbon-based materials with a pore space that contains pores of irregular shapes and sizes that follow a certain PSD. The pore networks are generated by the Voronoi tessellation of a solid material composed of millions to hundreds of thousands of atoms, and by designating a fraction of the Voronoi polyhedra as the pores. The pore space of many natural porous materials, ranging from biological materials, wood, and foam (Gibson and Ashby, 1997; Unger et al., 1988), to sandstone and other types of rock (Sahimi, 1995), can be well represented by Voronoi-type structures. The model allows for the investigation of the effect of the morphology on the pore space, i.e., its PSD and pore connectivity, on the adsorption and transport of methane and CO_2 for capture and storage applications (Firouzi and Wilcox, 2012, 2013).

Techniques to determine pore size distributions include small angle X-ray scattering (SAXS) and small angle neutron scattering (SANS) (Radlinski et al., 2004) and ^{129}Xe NMR (Terskikh et al., 1993). In this study, we utilize proton NMR cryoporometry and low-pressure gas adsorption isothermal experiments to characterize the porous structure of two reference materials, lignite coal and gas shale. NMR cryoporometry detects the pore-size-dependent shift of the melting and/or freezing points of pore imbibed materials (Hansen et al., 1996; Petrov and Furó, 2006; Strange et al., 1993). For detection, NMR cryoprometry exploits the substantial difference between solid and liquid NMR signals. In the gas adsorption experiments, isotherms were developed using N_2 as the probe gas with a Quantachrome Autosorb iQ_2 instrument. The isotherms were then analyzed to determine the PSD and total micro- and mesopore volumes of the coal and gas shale samples.

In the first part of this work, the molecular pore network simulation employed to model the carbon-based porous structure of coals and gas shales is described. Next, the NMR cryoporometry and gas adsorption techniques used to characterize the porous structure of reference materials and coal and gas shale are explained. The results are presented and analyzed in the final part.

2. Molecular porous structure model

The molecular pore network is generated based on geometric considerations alone and the chemical and energetic details of creating the pores are ignored. In this method, we begin with a 3-D cell of carbon atoms with a structure corresponding to graphite so that the number density of carbon atoms is 114 nm^{-3} and the spacing between the adjacent graphene layers in the z- direction is 0.335 nm. Periodic boundary conditions were employed in all directions. The details of the system size are elucidated in the results and discussion section. The graphite cell is then tessellated through the insertion of a given number of Poisson points at random positions inside the simulation cell, each of which is used for constructing a 3-D Voronoi polyhedron, such that every point inside each polyhedron is closer to its own Poisson point than to any other Poisson point. The pore space is then generated by fixing the desired porosity and selecting a number of polyhedra, that can be chosen randomly or by first sorting and listing the polyhedra in the cell according to their sizes from smallest to largest (or vice versa), in such a way that their total volume fraction equals the desired porosity. The polyhedra, so chosen, are then designated as the pores by removing the carbon atoms comprising them, as well as those that are connected to only one neighboring carbon atom (the dangling atoms, i.e., connected to only one other atom), since it is impossible to have such atoms connected to the internal surface of the pores. Also, removal of the dangling atoms gives rise to pore surface roughness at the molecular level, which is expected to exist in any real pore (Firouzi and Wilcox, 2012; Rajabbeigi et al., 2009a,b; Xu et al., 2000a). The remaining carbon atoms constitute the solid matrix, while the pore space consists of interconnected pores of various shapes and sizes. We should note that the influence of heteroatoms is not included in this work. The equivalent radius size of each polyhedron is taken to be the radius of a sphere that has the same volume as the polyhedron.

If the pore polyhedra are selected at random, then, assuming that the size of the simulation cell is large enough, their size distribution will always be Gaussian, regardless of the porosity or even the size of the initial graphite cell. The 3-D graphite pore networks with desired porosities can be generated using this model. In addition, any desired average pore size can be fixed by varying the number of Poisson points inside the initial graphite cell. Clearly, the larger the number of Poisson points, the smaller the average pore size. The pore space generated by these models is a molecular-scale pore network and, unlike the traditional pore networks that are used in the simulation of flow and transport in microporous media, this allows for the interaction of the fluid molecules with the atoms in the structure. Moreover, the Voronoi algorithm has great flexibility in terms of constructing disordered pore networks with many variations in the sizes and shapes of the polyhedra. The algorithm can be modified to generate pore polyhedra with a great variety of shapes, from completely random to very regular shapes (Cromwell, 1997).

The Voronoi network has been previously utilized as a prototype of irregular networks to study transport in disordered composites (Jerauld et al., 1984a,b; Sahimi and Tsotsis, 1997), and the statistics of Voronoi tessellations have been used in the past to characterize the porosity distribution in porous materials (Dominguez and Rivera, 2002; Firouzi and Wilcox, 2012, 2013; Ghassemzadeh et al., 2000; Rivera and Dominguez, 2003; Xu et al., 2000a, 2001). The Voronoi structure has also been used in the past for modeling of polymer membrane and adsorption processes. The atomistic Voronoi structure has been developed to model carbon membranes to study the transport and adsorption of gases, including the existence of an optimal pore structure for maximum gas separation (Xu et al., 2000a). The Voronoi model has also been utilized to compute the adsorption isotherms of N_2 in three distinct silicon-carbide (SiC) membranes at 77 K, and transport and separation of H_2/CO_2 and H_2/CH_4 mixtures and found reasonable agreement with experimental data (Rajabbeigi et al., 2009a,b). In addition, previous studies included a comparison of the computed PSD for the model Carbon Molecular Sieve Membrane (CMSM) using the Voronoi tessellation to the experimentally measured PSD of a typical CMSM (Xu et al., 2000b), which are in reasonable agreement (Firouzi, 2005).

3. Characterization experiments

Reference materials used were a silica gel, SiliaFlash F60 (SiliCycle, Inc., Canada) of 230–400 mesh particle size and 60 Å pore size, and an open-cell porous glass, Vycor 7930 (Corning, Inc., New York) of 30–100 mesh particle size and 40 to 200 Å pore diameter. The coal sample used in the studies is a wet, lignite sample from North Dakota, United States. The shale sample is from the Eagle Ford shale formation from southeast Texas, United States. The formation is characterized as a “black” or organic-rich shale.

The SiliaFlash F60 and Vycor 7930 reference materials were used as provided. The lignite and shale samples were prepared by grinding a representative sample (0.1 to 0.2 g) in a chalcedony mortar and pestle and sieved through a 45-mesh (Tyler equivalent) screen so the entire

sample consisted of particles with at least two dimensions less than 354 μm.

3.1. NMR cryoporometry experiments

NMR samples were prepared by placing dry material to a depth of approximately 2–5 mm at the bottom of 5-mm (outer diameter) NMR tubes. The tubes were filled with distilled, deionized water and manually agitated to eliminate clumping. The tubes were gently spun in a centrifuge at room temperature for a minimum of 12 h to help saturate the materials. Tubes were occasionally removed from the centrifuge to manually agitate the materials. Prior to NMR analysis, the majority of the water from the tubes was pipetted out leaving a minimal head of water over the surface of the material. The ^{1}H NMR cryoporometric experiments were carried out on a Varian Inova 600 MHz spectrometer running VNMR 6.1C, equipped with a conventional 5-mm probe (H{CN}, z-axis gradient), and variable sample temperature controller. The system temperature was calibrated with a 100% MeOH temperature calibration standard sample. NMR tubes were positioned to center the material in the middle of the probe coil. A CPMG spin-echo sequence was used to detect a liquid water signal and to suppress a solid ice signal (Sagidullin and Furó, 2008) with 4 spin echoes of 40 ms total echo time. The sample temperature was first equilibrated to 1 °C in the temperature controlled NMR probe for 1–2 h, then the probe was tuned, ^{1}H 90° pulse width was calibrated, and the experimental receiver gain was optimized based on the bulk water signal. The samples were not shimmed and the lock was turned off. Sample temperatures were then lowered to −20 °C (−15 °C for the Vycor 7930) to freeze all of the water. Test experiments were acquired at this low temperature to determine if any liquid water signal was still observable (due to the freezing point depression of water in small pores). If so, samples were removed from the spectrometer, soaked in liquid nitrogen for 10–15 min, and quickly returned to the −20 °C or −15 °C regulated NMR probe. Samples were held at the low temperature (−20 °C or −15 °C) for a number of hours to ensure sample temperature equilibration. Sample temperatures were increased in 0.1 °C increments until all ice in the samples had melted. The samples would spend 40 min (20 min for Vycor 7930) at each increment to equilibrate temperature and acquire the CPMG spin-echo detection experiment (typically with 80,000 Hz spectral width, 16,384 total data points, 64–2048 scans per increment). Data were processed on the spectrometer with line-broadening of 100 Hz signal integrated per increment. PSDs were determined via a modified form of the Gibbs–Thompson equation as described by others (Petrov and Furó, 2006; Sagidullin and Furó, 2008).

3.2. Low pressure gas adsorption

Gas adsorption isotherms were developed on each of the samples using a Quantachrome Autosorb iQ_2 instrument. The samples were outgassed at 110 °C for 60 min and then held at 140 °C for 180 min at a pressure of 1×10^{-3} bar. The purpose of the outgas procedure is to drive off H_2O and other adsorbed gases, which may impact the isotherm, without materially impacting the shale and coal samples. At the end of the outgas procedure, the sample was tested for continued outgassing, to ensure completion. Complete outgassing was verified for each sample. In related initial work, this outgas procedure has been observed to be the bare minimum required to provide semi-repeatable isotherms that are appropriate for further analysis. Research into the proper preparation procedure for low-pressure adsorption on shale samples is ongoing, and further improvements in the technique are necessary. However, this method provides an appropriate platform to compare experimental and computational methods.

The isotherms were performed at 77 K (held constant with a liquid N_2 bath) with 99.999% N_2 used as the probe gas. Adsorption isotherms were performed with 47 points in a range of $1.0 \times 10^{-7} \leq P/P_0 \leq 0.995$ with an equilibrium time of 8 min, allowing the sample to reach a near-equilibrium state. A 20-point desorption isotherm was also performed from $0.05 \leq P/P_0 \leq 0.995$. The PSDs were created using an included density function theory method, with the method choice being determined by a combination of probe gas, adsorbent surface, pore shape and isotherm fit. The method chosen for the natural samples, quenched solid density functional theory (QSDFT) (Gor et al., 2012), used N_2 on carbon at 77 K assuming a combination of slit and cylindrical pores, which correctly take into account the metastability of the pore fluid. The QSDFT method was chosen due to correctness of fit, as evaluated by the Quantachrome software and compared to a QSDFT method assuming slit pores only. In addition, prior imaging (Bai et al., 2013; Curtis et al., 2011) on a variety of shale samples has indicated that the organic matter has a range of pore geometries, including slit, cylindrical and amorphous shapes, indicating a slit pore-only method would insufficiently model the PSD. A method based on non-localized density functional theory (NLDFT) (Neimark and Ravikovitch, 2001), assuming cylindrical pores and N_2 adsorption on silica at 77 K, was used for the SiliaFlash F60 and Vycor 7930 samples. Both methods are based on the adsorption isotherm using the entire P/P_0 range, which can be seen for each material in Fig. 1. The desorption isotherm for each sample can also be seen in Fig. 1. The silica samples had Type IV isotherms, as expected based on published pore sizes for the materials. Total pore volume is calculated using the Gurvich rule (Lowell et al., 2004).

4. Results and discussion

The PSDs determined by low-pressure gas adsorption for SiliaFlash F60 and Vycor 7930 are shown in Fig. 2. The average pore diameter for SiliaFlash F60 was found to be 6 nm, with a total pore volume of 6.65×10^{-1} cm^3/g. The Vycor 7930 had a smaller total pore volume of 2.21×10^{-1} cm^3/g with an average pore diameter of approximately 11 nm. The corresponding PSD fits from the NMR cryoporometry are shown in Fig. 3, where the PSDs for SiliaFlash F60 and Vycor 7930 were found to be 3–7 nm and 6–9 nm, respectively. The PSDs determined on these reference materials show a reasonable agreement between low-pressure gas adsorption and NMR cryoporometry techniques demonstrating agreement and consistency between the two independent methods.

The NMR cyroporometry could not determine the PSDs of the coal and shale samples. The NMR melt curves only observed the bulk water melt allowing no basis for PSD fitting. This is likely a function of the pore surface chemistry and pore size, where much lower temperature than predicted by the Gibbs–Thompson Equation is needed to completely freeze the water inside the pores (Allardice et al., 2003; Ghosh et al., 2004; Mraw and Naas-O'Rourke, 1979); temperatures that could not be achieved by the NMR instrumentation used. The SiliaFlash F60 and Vycor 7930 pore water melted at approximately 260 K and 265 K, respectively, within the temperature range for the NMR cryoporometry trials performed. However Norinaga et al. (1998, 1999) examined a number of coal samples by DSC and NMR spin-echo relaxation techniques and found that freezing of pore water occurred between 260 and 213 K and a fraction of the water remained non-freezable well below 213 K. Additionally, Ghosh et al. (2004) examined single-walled carbon nanotubes by NMR line-shape analysis to find that freezing occurred in two steps, at 242 K for water in the center core of the nanotubes, and at 212 K for the water shell around the center core water. These temperatures would have been below the range possible with the available NMR instrumentation.

Previous studies have shown a shift in melting points of water depending upon the pore size (Jähnert et al., 2008; Sagidullin and Furó, 2008). The current work indicates that for pores on the order of 10s of nanometers or less, the surface chemistry of the pore begins to play a role on the phase behavior of the confined fluid. It is important to note that the probability of water freezing in a pore is dependent on the relative fluid–fluid versus fluid-pore wall interactions. In some materials, water may interact with the surface in a geometrically constricted

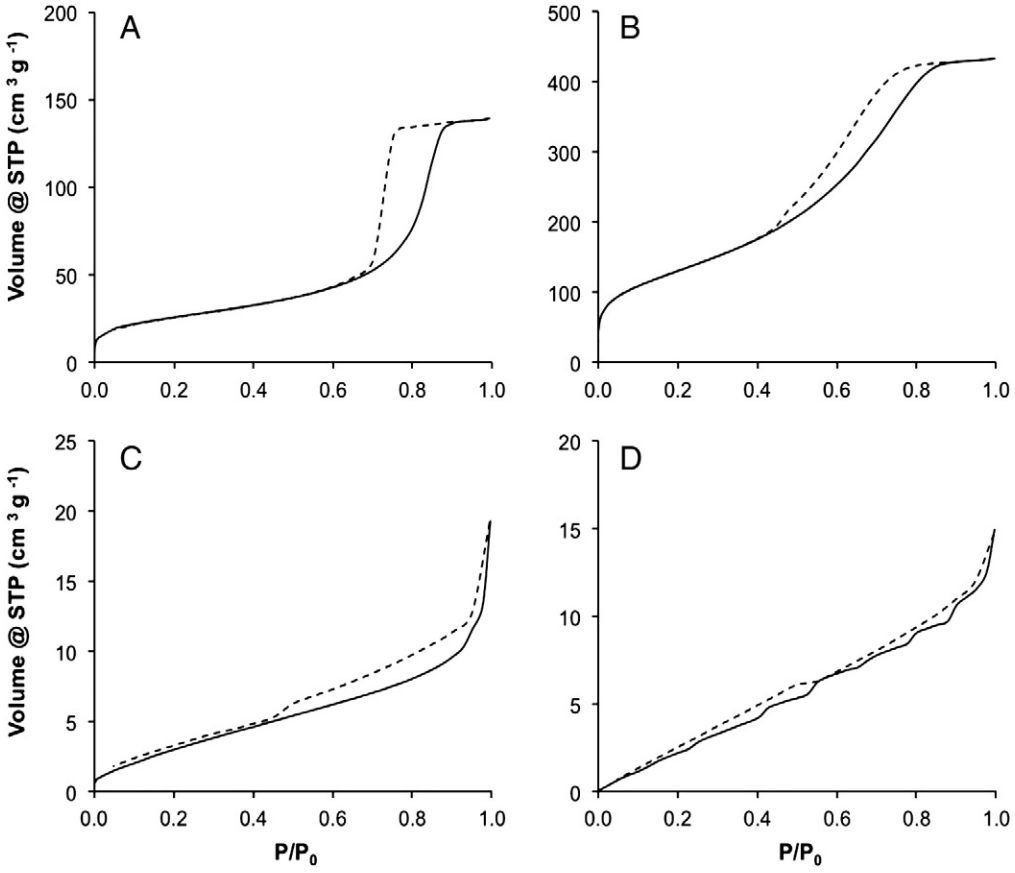

Fig. 1. N_2 adsorption (solid) curves and desorption (dashed) curves isotherms for: Reference materials Vycor 7930 (A) and SiliaFlash F60 (B), and natural materials Eagle Ford shale (C) and lignite coal (D).

fashion, making it difficult to form the tetrahedral coordination required for the formation of ice at the pore surface. However, depending upon the width of the pore, ice may be able to form in the center of the pore, provided the pore walls are far enough apart so that the coordination is not impacted significantly. Additionally, materials may exist in which water has limited interactions with the pore surface, thereby leading to a surface layer that resembles ice (Coasne et al., 2013). The pores of the natural materials considered in the current work are complex mixtures of kerogen and clay and their surface chemistry clearly plays a role in the extent to which ice is able to form, thereby limiting the NMR cryoporometry method for determining PSD in these materials.

Molecular simulations of 3-D carbon-based porous networks were carried out and benchmarked by successful PSD measurements of the low-pressure gas adsorption experiments to represent the micro and mesoporous structure of the complex coal and gas shale samples. Fig. 4 shows a comparison between the predicted and the experimentally

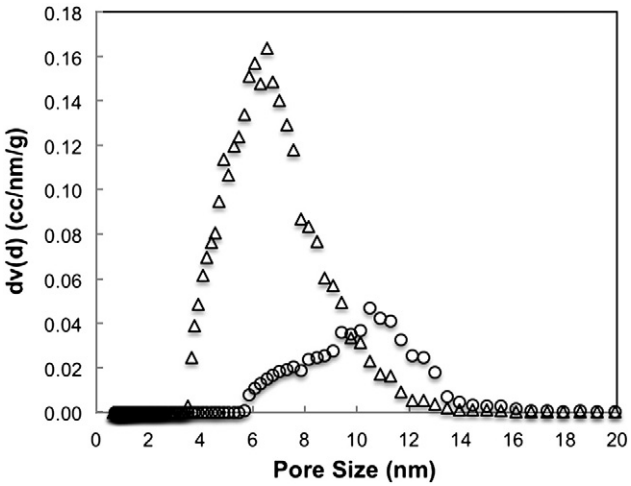

Fig. 2. PSD determined by low-pressure gas adsorption isotherms for reference material SiliaFlash F60 (triangles) and Vycor 7930 (circles).

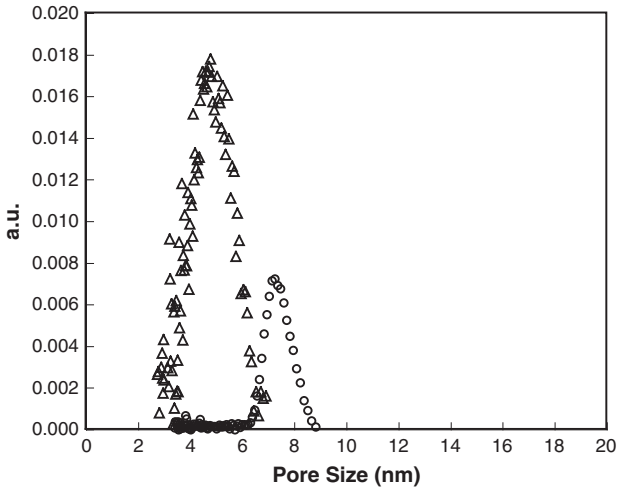

Fig. 3. PSD determined by NMR cryoporometry for reference materials SiliaFlash F60 (triangles) and Vycor 7930 (circles). SiliaFlash F60 was found to have a range of pore sizes from 3 to 7 nm. Vycor 7930 was found to have a range of pore sizes from 6 to 9 nm. Y-axis is in arbitrary units (a.u.). The two traces have been scaled to aid visual comparison to Fig. 1.

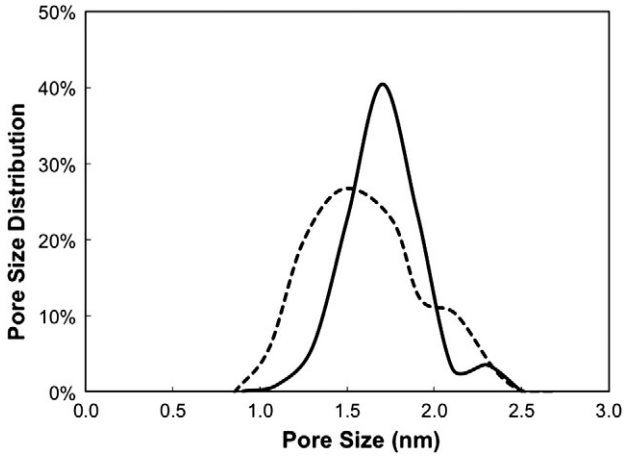

Fig. 4. Computed PSD of the pore network (solid curve) and PSD determined by low-pressure gas adsorption (dotted curve) for Eagle Ford shale.

measured PSD of the Eagle Ford shale sample. In Fig. 4, the size of the initial graphite cell in the modeling is 102, 103, and 103 Å in x-, y-, and z- directions, respectively. The carbon atoms were packed with 31 layers of graphene. The total initial number of carbon atoms in each graphene layer and the simulation cell were 4032 and 124,992 respectively. The porosity is 15% and the pores are selected randomly, with average pore sizes of 1.6 nm. The number of inserted Poisson points in the simulation cell is 460 and the total number of carbon atoms in generated pore network matrix is 105,813. The PSDs and their averages that are generated resemble the experimental PSD obtained for the Eagle Ford sample using gas adsorption. As can be seen in Fig. 4, the experimental PSD for the Eagle Ford sample also shows a peak around 1.5 nm.

Fig. 5 shows a comparison between the predicted and experimentally measured PSD of the North Dakota lignite coal sample. In Fig. 5 the size of the initial graphite cell in our modeling is 302, 303, and 301 Å in x-, y-, and z- directions, respectively. The carbon atoms were packed with 90 layers of graphene. The total initial number of carbon atoms in each graphene layer and the simulation cell were 34,932 and 3,143,880 respectively. The porosity is 15% and the pores are selected randomly, with average pore sizes of 5.0 nm. The number of inserted Poisson points in the simulation cell is 380 and the total number of carbon atoms in the generated pore network matrix is 2,673,343. The PSDs and their averages that are generated resemble the experimental PSD obtained for lignite by gas adsorption. It is important to note that the experimental distributions presented in Figs. 4 and 5 are a small portion

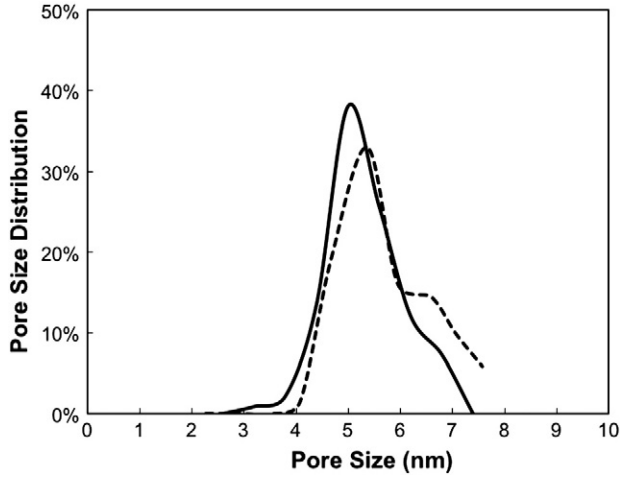

Fig. 5. Computed PSD of the pore network (solid curve) and PSD determined by low-pressure gas adsorption (dotted curve) for North Dakota lignite.

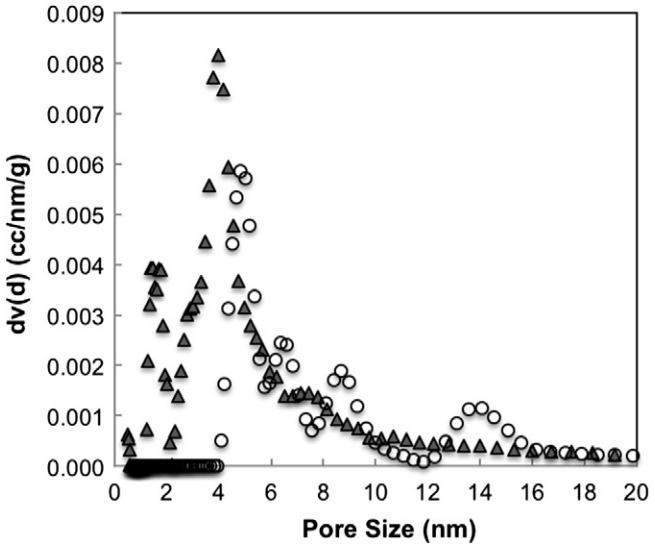

Fig. 6. PSD determined by low-pressure gas adsorption isotherms for Eagle Ford shale (solid triangles) and North Dakota lignite (circles).

of the complete distribution, which can be seen in Fig. 6. The natural samples do not have as well as a defined pore structure as the silica samples, thus showing a wider distribution of pore sizes. It should also be noted that the total experimental pore volume for these samples was much less than for the silica samples, with the lignite and shale samples at 2.31×10^{-2} and 3.70×10^{-2} cm^3/g, respectively.

5. Conclusions

Characterization experiments of NMR cryoporometry and low-pressure N_2 adsorption isotherms have been carried out to understand PSD and porosity that will provide insight into the development of realistic simulation models for the organic matter comprising coal and gas shales. We find that PSDs of reference compounds determined by NMR cryoporometry and N_2 isotherms from low-pressure gas adsorption were consistent, demonstrating the complementary nature of the two techniques. This gave confidence in use of the lignite and shale PSDs determined by gas adsorption as benchmarks for the molecular simulations performed.

The inability to measure PSDs in coal and shales (micro and mesoporous materials) using NMR cryoporometry is likely due to both pore size and pore surface chemistry. The available NMR instrumentation could not scan temperatures lower than 253 K, which capped the pore sizes that could be studied (a situation we are seeking to remedy, as NMR cryoporometry can be a valuable tool to probe pore size distributions as a complement to data from other techniques). However it is important to note that in the experiments carried out, the pore sizes of the coal and shale samples investigated and used for benchmarking the molecular simulation studies primarily ranged between 1 and 6 nm, while the silica-based materials had pore sizes ranging between approximately 3 to 12 nm. Although the pore sizes measured in the silica-based materials were generally larger, overlap in pore sizes among the different types of samples existed, indicating that size alone does not explain the temperature shift and inability to freeze the water at the conditions of the NMR experiments in this work. This suggests that the pore surface chemistry likely plays a role in nanoscale material. For instance, water may be more densely packed in a silica-based pore, where hydrogen bonding with the pore walls is likely to lead to a condensed phase more readily than a carbon-based wall at the same temperature. Future work will involve density estimates of pores with silica- versus carbon-based pore walls as a function of temperature and pore size, which will allow this hypothesis to be tested.

Molecular simulation studies were applied to model the porous structure of the lignite and gas shale samples. The 3-D pore network model was generated atomistically using the Voronoi tessellation method of a structure containing millions to hundred thousands of atoms. A comparison of the computed PSD was made to the PSDs determined from experimental adsorption isotherms using DFT methods of typical coal and shale, and are in reasonable agreement. More complex molecular models will be investigated to model the real structure of coal and gas shale rocks considering the vacancies and functional groups of the pore surfaces. Knowing the PSD, porosity and pore connectivity will lead to the predictability of transport and storage possibilities for enhanced methane recovery along with potential CO_2 sequestration in coal and gas shales.

Acknowledgments

We are grateful to the Department of Energy — National Energy Technology Laboratory for partial support of this work. The computations were carried out on the Center for Computational Earth & Environmental Science (CEES) cluster at Stanford University. Also, we would like to thank Dennis Michael for helping us to install our codes onto CEES.

References

Allardice, D.J., Clemow, L.M., Favas, G., Jackson, W.R., Marshall, M., Sakurovs, R., 2003. The characterisation of different forms of water in low rank coals and some hydrothermally dried products. Fuel 82 (6), 661–667.
Bai, B., Elgmati, M., Zhang, H., Wei, M., 2013. Rock characterization of Fayetteville shale gas plays. Fuel 105, 645–652.
Coasne, B., Galarneau, A., Pellenq, R.J.M., Renzo, F.D., 2013. Adsorption, intrusion and freezing in porous silica: the view from the nanoscale. Chem. Soc. Rev. 42, 4141–4171.
Cromwell, P.R., 1997. Polyhedra. Cambridge University Press, Cambridge.
Curtis, M.E., Ambrose, R.J., Sondergeld, C.H., Rai, C.S., 2011. Investigation of the Relationship between Organic Porosity and Thermal Maturity in the Marcellus Shale in SPE North American Unconventional Gas Conference and Exhibition (The Woodlands, TX, USA) (SPE 144370).
Dominguez, H., Rivera, M., 2002. Studies of porosity and diffusion coefficient in porous matrices by computer simulations. Mol. Phys. 100 (24), 3829–3838.
Faulon, J.L., Hatcher, P.G., Carlson, G.A., Wenzel, K.A., 1993. Fuel Process. Technol. 34, 277–293.
Firouzi, M., 2005. Molecular simulation of the structure, transport, and separation of fluid mixtures in nanoporous membranes under subcritical and supercritical conditions (Ph.D. dissertation).
Firouzi, M., Wilcox, J., 2012. Molecular modeling of carbon dioxide transport and storage in porous carbon-based materials. Microporous Mesoporous Mater. 158, 195–203.
Firouzi, M., Wilcox, J., 2013. Slippage and viscosity predictions in carbon micropores and their influence on CO_2 and CH_4 transport. J. Chem. Phys. 138, 064705 (12 pages).
Ghassemzadeh, J., Xu, L., Tsotsis, T.T., Sahimi, M., 2000. Statistical mechanics and molecular simulation of adsorption in microporous materials: pillared clays and carbon molecular sieve membranes. J. Phys. Chem. B 104 (16), 3892–3905.
Ghosh, S., Ramanathan, K.V., Sood, A.K., 2004. Water at nanoscale confined in single-walled carbon nanotubes studied by NMR. Europhys. Lett. 65 (5), 678–684.
Gibson, L.J., Ashby, M.F., 1997. Cellular Solids: Structure and Properties, 2nd ed. Cambridge University Press, Cambridge.
Gor, G.Y., Thommes, M., Cychosz, K.A., Neimark, A.V., 2012. Quenched solid density functional theory method for characterization of mesoporous carbons by nitrogen adsorption. Carbon 50 (4), 1583–1590.
Hansen, E.W., Schmidt, R., Stöcker, M., 1996. Pore structure characterization of porous silica by ^{1}H NMR using water, benzene, and cyclohexane as probe molecules. J. Phys. Chem. 100 (27), 11396–11401.
International Union of Pure and Applied Chemistry (IUPAC), 1972. Manual of Symbols and Terminology for Physico Chemical Quantities and Units. Butterworth, London, U.K.
IPCC Fourth Assessment Report (AR4), 2007. Climate Change: The Physical Science Basis. IPCC.
Jähnert, S., Chávez, F.V., Schaumann, G.E., Schreiber, A., Schönhoff, M., Findenegg, G.H., 2008. Melting and freezing of water in cylindrical silica nanopores. Phys. Chem. Chem. Phys. 10, 6039–6051.
Jerauld, G.R., Hatfield, J.C., Scriven, L.E., Davis, H.T., 1984a. Percolation and conduction on Voronoi and triangular networks: a case study in topological disorder. J. Phys. C Solid State Phys. 17, 1519–1529.
Jerauld, G.R., Scriven, L.E., Davis, H.T., 1984b. Percolation and conduction on the 3D Voronoi and regular networks: a second case study in topological disorder. J. Phys. C Solid State Phys. 17, 3429–3439.
Lowell, S., Shields, J.E., Thomas, M.A., Thommes, M., 2004. Characterization of Porous Solids and Powders: Surface Area, Pore Size and Density. Springer, The Netherlands.
Mraw, S.C., Naas-O'rourke, D.F., 1979. Water in coal pores — low-temperature heat-capacity behavior of the moisture in Wyodak coal. Science 205 (4409), 901–902.
Neimark, A.V., Ravikovitch, P.I., 2001. Capillary condensation in MMS and pore structure characterization. Microporous Mesoporous Mater. 44–45, 697–707.
Norinaga, K., Kumagai, H., Hayashi, J.-i., Chiba, T., 1998. Classification of water sorbed in coal on the basis of congelation characteristics. Energy Fuel 12 (3), 574–579.
Norinaga, K., Hayashi, J.-i., Kudo, N., Chiba, T., 1999. Evaluation of effect of predrying on the porous structure of water-swollen coal based on the freezing property of pore condensed water. Energy Fuel 13 (5), 1058–1066.
Petrov, O., Furó, I., 2006. Curvature-dependent metastability of the solid phase and the freezing–melting hysteresis in pores. Phys. Rev. E. 73, 011608 (7 pages).
Radlinski, A.P., Mastalerz, M., Hinde, A.L., Hainbuchner, M., Rauch, H., Baron, M., Lin, J.S., Fan, L., Thiyagarajan, P., 2004. Application of SAXS and SANS in evaluation of porosity, pore size distribution and surface area of coal. Int. J. Coal Geol. 59 (3–4), 245–271.
Rajabbeigi, N., Elyassi, B., Tsotsis, T.T., Sahimi, M., 2009a. Molecular pore-network model for nanoporous materials. I: application to adsorption in silicon–carbide membranes. J. Membr. Sci. 335, 5–12.
Rajabbeigi, N., Tsotsis, T.T., Sahimi, M., 2009b. Molecular pore-network model for nanoporous materials. II: application to transport and separation of gaseous mixtures in silicon–carbide membranes. J. Membr. Sci. 345, 323–330.
Rivera, M., Dominguez, H., 2003. Pore matrices prepared at supercritical temperature by computer simulations: matrix characterization and studies of diffusion coefficients of adsorbed fluids. Mol. Phys. 101 (19), 2953–2962.
Sagidullin, A.I., Furó, I., 2008. Pore size distribution measurements in small samples and with nanoliter volume resolution by NMR cryoporometry. Langmuir 24 (9), 4470–4472.
Sahimi, M., 1995. Flow and Transport through Porous Media and Fractured Rock. VCH, Weinheim.
Sahimi, M., Tsotsis, T.T., 1997. Transient diffusion and conduction in heterogeneous media: beyond the classical effective-medium approximation. Ind. Eng. Chem. Res. 36 (8), 3043–3052.
Sharkey Jr., A.G., McCartney, J.T., 1981. In: Elliott, M.A. (Ed.), Chemistry of Coal Utilization, second supplementary volume. Wiley, New York, pp. 159–283.
Strange, J.H., Rahman, M., Smith, E.G., 1993. Characterization of porous solids by NMR. Phys. Rev. Lett. 71, 3589–3591.
Terskikh, V.V., Mudrakovskii, I.L., Mastikhin, M., 1993. ^{129}Xe nuclear magnetic resonance studies of the porous structure of silica gels. J. Chem. Soc. Faraday Trans. 89 (23), 4239–4243.
Unger, K.K., Rouquerol, J., Sing, K.S.W., Kral, H. (Eds.), 1988. Characterization of Porous Solids. Elsevier, Amsterdam.
Wang, F.Y., Zhu, Z.H., Massarotto, P., Rudolph, V., 2007. A simplified dynamic model for accelerated methane residual recovery from coals. Chem. Eng. Sci. 62 (12), 3268–3275.
White, C.M., Smith, D.H., Jones, K.L., Goodman, A.L., Jikich, S.A., LaCount, R.B., DuBose, S.B., Ozdemir, E., Morsi, B.I., Schroeder, K.T., 2005. Sequestration of carbon dioxide in coal with enhanced coalbed methane recovery—a review. Energy Fuel 19, 659–724.
Wilcox, J., 2012. Carbon Capture. Springer, New York.
Xu, L., Tsotsis, T.T., Sahimi, M., 2000a. Nonequilibrium molecular dynamics simulations of transport and separation of gas mixtures in nanoporous materials. Phys. Rev. E. 62 (5), 6942–6948.
Xu, L., Sedigh, M.G., Tsotsis, T.T., Sahimi, M., 2000b. Nonequilibrium molecular dynamics simulation of transport and separation of gases in carbon nanopores. II. Binary and ternary mixtures and comparison with the experimental data. J. Chem. Phys. 112 (2), 910–922.
Xu, L., Tsotsis, T.T., Sahimi, M., 2001. Statistical mechanics and molecular simulation of adsorption of ternary gas mixtures in nanoporous materials. J. Chem. Phys. 114 (16), 7196–7210.